2015

Seasonality of biological and physical controls on surface ocean CO2 from hourly observations at the Southern Ocean Time Series site south of Australia

EH Shadwick
Virginia Institute of Marine Science

TW Trull

B Tilbrook

AJ Sutton

E Schulz

See next page for additional authors

AGU PUBLICATIONS

Global Biogeochemical Cycles

RESEARCH ARTICLE

10.1002/2014GB004906

Key Points:
- Novel CO_2 and hydrographic time series from open Southern Ocean site
- Biology controls seasonal CO_2; deep mixing/winter respiration close annual cycle
- Small seasonal warming and prolonged biology drive net atmospheric CO_2 uptake

Correspondence to:
E. H. Shadwick,
shadwick@vims.edu

Citation:
Shadwick, E. H., T. W. Trull, B. Tilbrook, A. J. Sutton, E. Schulz, and C. L. Sabine (2015), Seasonality of biological and physical controls on surface ocean CO_2 from hourly observations at the Southern Ocean Time Series site south of Australia, *Global Biogeochem. Cycles*, *29*, 223–238, doi:10.1002/2014GB004906.

Received 29 MAY 2014
Accepted 18 JAN 2015
Accepted article online 24 JAN 2015
Published online 27 FEB 2015

Seasonality of biological and physical controls on surface ocean CO_2 from hourly observations at the Southern Ocean Time Series site south of Australia

E. H. Shadwick[1,2], T. W. Trull[1,3], B. Tilbrook[1,3], A. J. Sutton[4,5], E. Schulz[6], and C. L. Sabine[5]

[1]Antarctic Climate and Ecosystems Cooperative Research Centre, University of Tasmania, Hobart, Tasmania, Australia, [2]Now at Virginia Institute of Marine Sciences, College of William and Mary, Gloucester Point, Virginia, USA, [3]CSIRO Oceans and Atmosphere, Hobart, Tasmania, Australia, [4]Joint Institute for the Study of the Atmosphere and Ocean, University of Washington, Seattle, Washington, USA, [5]Pacific Marine Environmental Laboratory, NOAA, Seattle, Washington, USA, [6]Centre for Australian Weather and Climate Research, Bureau of Meteorology, Melbourne, Victoria, Australia

Abstract The Subantarctic Zone (SAZ), which covers the northern half of the Southern Ocean between the Subtropical and Subantarctic Fronts, is important for air-sea CO_2 exchange, ventilation of the lower thermocline, and nutrient supply for global ocean productivity. Here we present the first high-resolution autonomous observations of mixed layer CO_2 partial pressure (pCO_2) and hydrographic properties covering a full annual cycle in the SAZ. The amplitude of the seasonal cycle in pCO_2 (~60 µatm), from near-atmospheric equilibrium in late winter to ~330 µatm in midsummer, results from opposing physical and biological drivers. Decomposing these contributions demonstrates that the biological control on pCO_2 (up to 100 µatm), is 4 times larger than the thermal component and driven by annual net community production of 2.45 ± 1.47 mol C m^{-2} yr^{-1}. After the summer biological pCO_2 depletion, the return to near-atmospheric equilibrium proceeds slowly, driven in part by autumn entrainment into a deepening mixed layer and achieving full equilibration in late winter and early spring as respiration and advection complete the annual cycle. The shutdown of winter convection and associated mixed layer shoaling proceeds intermittently, appearing to frustrate the initiation of production. Horizontal processes, identified from salinity anomalies, are associated with biological pCO_2 signatures but with differing impacts in winter (when they reflect far-field variations in dissolved inorganic carbon and/or biomass) and summer (when they suggest promotion of local production by the relief of silicic acid or iron limitation). These results provide clarity on SAZ seasonal carbon cycling and demonstrate that the magnitude of the seasonal pCO_2 cycle is twice as large as that in the subarctic high-nutrient, low-chlorophyll waters, which can inform the selection of optimal global models in this region.

1. Introduction

The Southern Ocean is an important region for the global carbon cycle, exerting a major influence on the uptake of both natural [e.g., *Metzl et al.*, 2006; *Takahashi et al.*, 2009; *Lenton et al.*, 2013] and anthropogenic carbon dioxide (CO_2) [e.g., *Sabine et al.*, 2004; *Khatiwala et al.*, 2013]. Present-day Southern Ocean carbon fluxes reflect both significant uptake of human-induced CO_2 emissions [*Sabine et al.*, 2004] and spatial variations in the balance between uptake and outgassing of natural CO_2 [e.g., *Takahashi et al.*, 2002; *Lovenduski et al.*, 2009; *Lenton et al.*, 2012]. Despite this importance to global climate, the Southern Ocean remains a region of considerable uncertainty with respect to its carbon budget [e.g., *Gruber et al.*, 2009], due to both unresolved variability at the seasonal time scale and strong disagreement among simulated seasonal cycles in global carbon models [*Lenton et al.*, 2013; *Resplandy et al.*, 2014].

In the Subantarctic Zone (SAZ), between the Subtropical and Subantarctic Fronts (Figure 1) [e.g., *Rintoul and Trull*, 2001], the uptake of CO_2 is driven by biological and physical processes, both of which exhibit changes over seasonal and shorter time scales [e.g., *Lenton et al.*, 2006; *Resplandy et al.*, 2014]. Deep convective mixing in winter (to depths greater than 500 m) in the SAZ results in the formation of oxygen-rich Subantarctic Mode Water (SAMW), which makes a significant contribution to the uptake and storage of anthropogenic CO_2 [*McNeil et al.*, 2001; *Sabine et al.*, 2004; *Sallée et al.*, 2012]. The equatorward spreading of SAMW supplies oxygen to ventilate the lower thermocline and delivers nutrients to fuel primary production in broad areas of the global ocean [e.g., *Sarmiento et al.*, 2004].

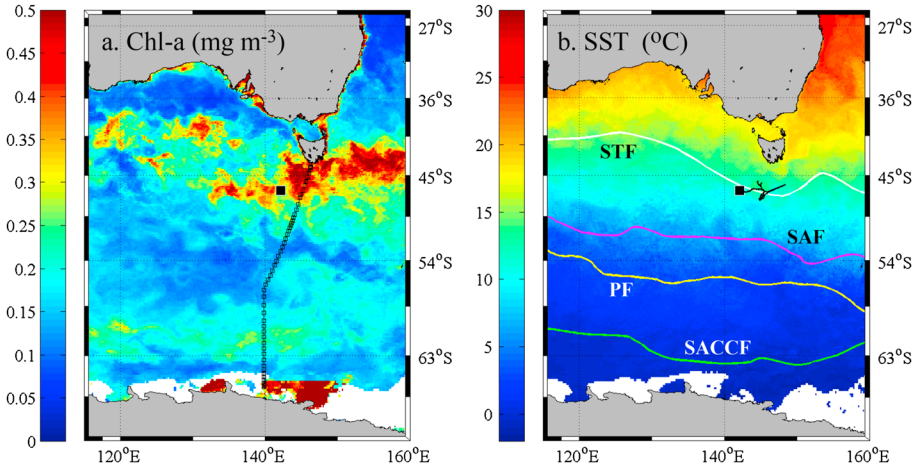

Figure 1. Maps of the study area showing (a) annual surface chlorophyll-a concentration and (b) annual sea surface temperature and the (climatological) locations of various Southern Ocean Fronts (following *Orsi et al.* [1995]): beginning in the north, the Subtropical Front (STF), the Subantarctic Front (SAF), the Polar Front (PF), and the Southern Antarctic Circumpolar Current (ACC) Front (SACCF). The location of the Southern Ocean Time Series (SOTS) station (46.8°S, 142°E) is indicated in both panels by the filled black square. The WOCE SR3 section is indicated by the open black squares in Figure 1a, and the location of the mooring during the (2012) drift period is shown by the black line in Figure 1b. The Subantarctic Zone (SAZ) is defined as the region between the STF and the SAF.

The Southern Ocean Time Series (SOTS) site (Figure 1) is located southwest of Tasmania, in the Indian/Australian sector of the SAZ, at a location that has been characterized as representative of a broader region of the SAZ between ~90°E and 140°E [*T. W. Trull et al.*, 2001]. The site is located between the eastward flowing Antarctic Circumpolar Current, concentrated along the Subantarctic Front (SAF) near 51°S, and the weaker westward flow of waters from the Tasman Sea to the north [*Herraiz-Borreguero and Rintoul*, 2011]. The environmental conditions at SOTS are temperate with seasonal mixed layer temperatures of ~9°C in winter and ~13°C in summer [*Rintoul and Trull*, 2001]. With respect to biogeochemical properties, this region of the SAZ is characterized by low to moderate chlorophyll (Figure 1a), relatively high nitrate and phosphate, and seasonal depletion of silicic acid [*Lourey and Trull*, 2001; *Rintoul and Trull*, 2001; *T. Trull et al.*, 2001]. Low concentrations of dissolved iron [*Bowie et al.*, 2009; *Lannuzel et al.*, 2011] likely limit summertime phytoplankton production in this region [*Sedwick et al.*, 1999]; but, nonetheless, the SAZ is one of the largest net sinks for atmospheric CO_2 at the annual scale [*Metzl et al.*, 1999; *Lenton et al.*, 2013], attributed in large part to the summertime biological control on surface water CO_2 concentrations [*Metzl et al.*, 1999, 2006; *McNeil and Tilbrook*, 2009].

Here we report the first full annual record of surface water CO_2 partial pressure (pCO_2) from an autonomous moored platform in the Southern Ocean. These high-frequency observations are used to partition seasonal changes in pCO_2 in the SAZ into physical and biological drivers and to assess the impact of short-term (i.e., subseasonal) hydrographic events on the biological carbon pump. Observations in the SAZ are compared to annual cycles of pCO_2 in high-nutrient, low-chlrophyll (HNLC) waters of the subarctic North Pacific, and important differences between the regions are identified. Given the appreciable role of the SAZ with respect to global biogeochemical cycling, this study, which identifies drivers of seasonal and shorter-term changes in the CO_2 system, has implications for assessments of natural variability in carbon cycling and CO_2 uptake in the broader global ocean.

2. Methods

2.1. Southern Ocean Time Series Observations

The Southern Ocean Time Series (SOTS) is part of the Australian Integrated Marine Observing System (IMOS), and consists of three deep ocean moorings [*Schulz et al.*, 2012; *Weeding and Trull*, 2014] in the SAZ at near 46.8°E and 142°S (Figure 1). The SAZ mooring is a stiff subsurface wire and glass float design that collects sinking particles into time series sediment traps in the deep ocean and has no instruments above 800 m depth [*T. Trull et al.*, 2001]. The Pulse mooring is an s-tether design with a small surface float that suspends a

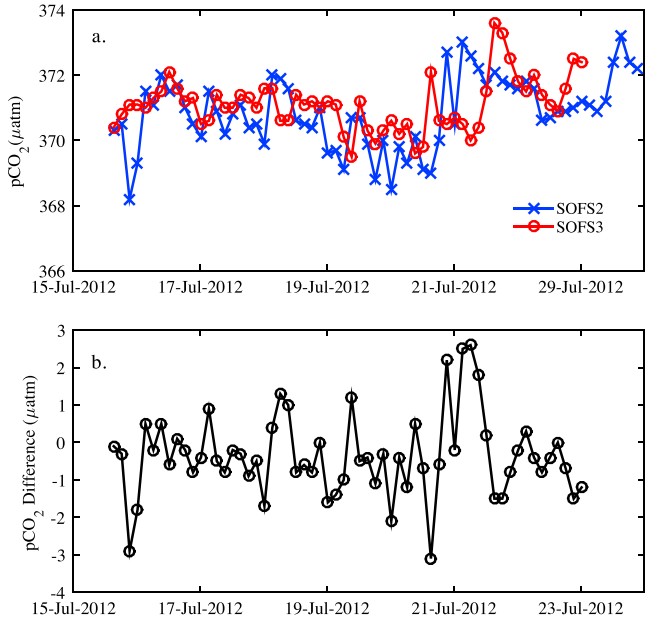

Figure 2. Between 15 and 23 July 2012, the SOFS 2 and SOFS 3 mooring deployments overlapped. (a) pCO_2 observations from both moorings over this period; (b) The pCO_2 difference.

package of biogeochemical sensors and a water sampler (RAS-500, Mclane, Inc.) in the surface mixed layer at ~35 m depth using elastic bungies to reduce movement of the instruments [*Pender et al.*, 2010; *Weeding and Trull*, 2014]. The Southern Ocean Flux Station (SOFS) mooring is a deep ocean polymer s-tether design, with a large surface float that supports a 3 m tower for meteorological measurements by dual ASIMET packages [*Schulz et al.*, 2012]. The ASIMET system measures humidity, sea surface and air temperature, and wind speeds (measured at a height of 3.17 m and scaled up by a factor of 1.1 for comparison to the standard 10 m height used in air-sea flux gas and heat flux computations) [*Schulz et al.*, 2012]. The moorings are serviced annually and their deployments numbered sequentially (e.g., SOFS 2, SOFS 3, Pulse 9, etc.). Hydrographic and atmospheric data from the SOTS moorings are publicly available via the IMOS Ocean Portal (http://imos.org.au).

Instruments attached to the surface buoy make ocean measurements of temperature, salinity, and pCO_2 (and also dissolved oxygen, phytoplankton fluorescence, and particulate backscatter); the instruments record conditions at approximately 1 m depth. Additional temperature and pressure loggers attached along a 800 m length of wire below the SOFS float provide data for the estimation of mixed layer depth (from measurements at 10, 20, 29, 40, 55, 60, 65, 70, 75, 85, 100, 110, 120, 140, 160, 200, 240, 280, 320, 360, 400, 440, and 480 m depth). Three criteria were applied for mixed layer depth estimation: a threshold of 0.3°C change from the surface temperature; a temperature gradient threshold of 0.005°C m^{-1}; and the maximum vertical temperature gradient, with the shallowest depth chosen [*Weeding and Trull*, 2014]. The SOFS-2 mooring had temperature sensors extending to only 160 m depth, and, fortunately, mixed layer depths were shallower than this during this spring/summer/autumn period.

The Moored Autonomous pCO_2 (MAPCO2) system measures the mole fraction of CO_2 in surface seawater (at approximately 0.5 m below the sea surface) and marine boundary air (at approximately 1.5 m above the sea surface) every 3 h, using an automated equilibrator-based gas collection system and nondispersive infrared gas analyzer [*Sutton et al.*, 2014]. These data, in addition to sample temperature, pressure and relative humidity, and sea surface temperature and salinity, are used to compute pCO_2 [*Weiss*, 1974; *Dickson et al.*, 2007]. Estimated uncertainty for MAPCO2 air and seawater pCO_2 measurements is better than 2 μatm [*Sutton et al.*, 2014]. The SOFS pCO_2 data are archived at the Carbon Dioxide Information Analysis Center (http://cdiac.ornl.gov/oceans/time_series_moorings.html).

We present results from three SOFS mooring deployments: SOFS2 from 24 November 2011 to 23 July 2012; SOFS 3 from 15 July 2012 to 2 January 2013; and SOFS 4 from 1 May 2013 to 14 October 2013. SOFS 2 data from the short overlapping period of 15–23 July 2012 are shown in Figure 2 and provide a useful reflection on pCO_2 accuracy and precision, with a mean pCO_2 difference between the two moorings of 0.74 μatm and standard deviation of 2 μatm. The analysis in this study is largely focused on the observations from 2012, with other data included to give a sense of the interannual variability in the hydrographic and CO_2 system parameters at the SOTS site. From 24 September to 31 December 2012, the SOFS 3 the mooring broke free and drifted eastward (see Figure 1b) into waters with similar surface water properties. Results from this period of drift are discussed in section 3.1. Performance characteristics of the ASIMET system are available in *Schulz et al.* [2012] and for the mixed layer depth loggers in *Weeding and Trull* [2014].

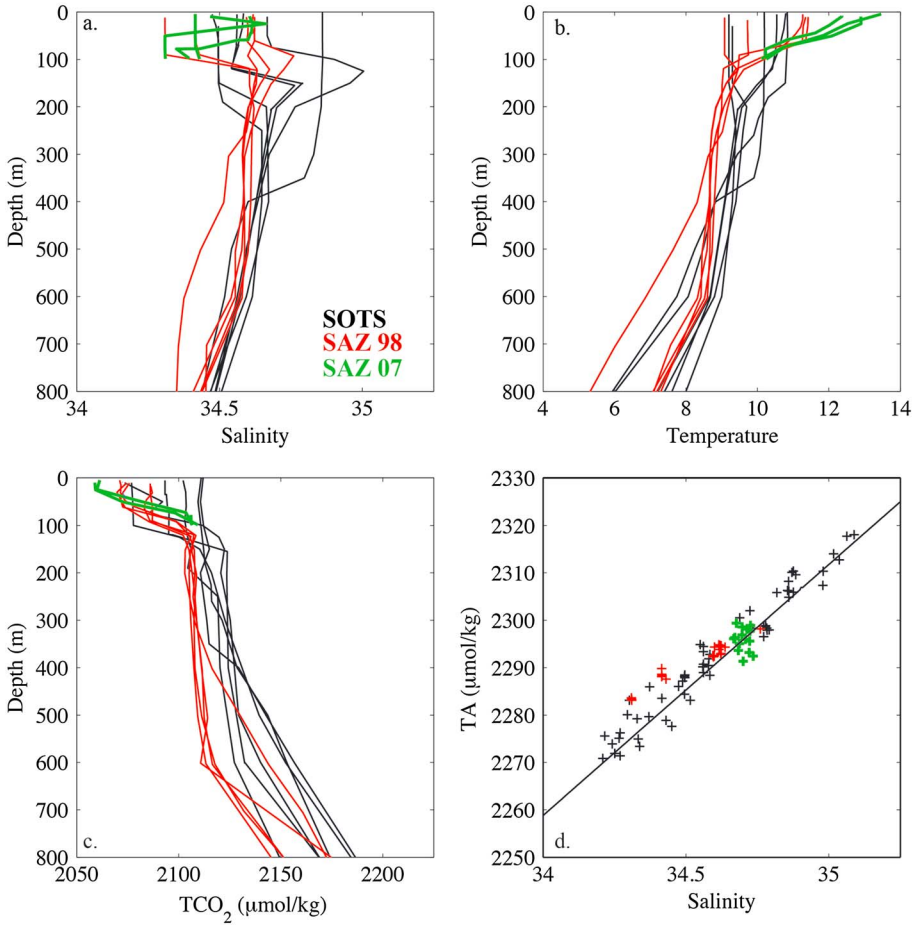

Figure 3. Upper ocean profiles of (a) salinity, (b) temperature, and (c) TCO_2 at the SOTS station. (d) The relationship between alkalinity (TA) and salinity (in the upper 400 m) used in the CO_2 system computations (TA = 53S + 460). Observations in black were collected at the SOTS station in March 2010, August 2011, July 2012, and May 2013; observations shown in red and green are from March 1998 and February 2007, respectively.

Surface chlorophyll-a, was obtained from the NASA MODIS-Aqua satellite [*Acker and Leptoukh*, 2007]; 8 day values in the region bounded by 46–48°E and 141–143°S were used to construct a seasonal cycle of chlorophyll for the year 2012 at the SOTS site. Surface silicate was obtained from the CSIRO Atlas of Regional Seas in the same location (CARS) (www.cmar.csiro.au/cars) [*Ridgway et al.*, 2002], which provides gridded fields of mean water properties and average (climatological) seasonal cycles generated from observations.

Additional, discrete observations of total dissolved inorganic carbon (TCO_2) and total alkalinity (TA) were collected on the RV *Southern Surveyor* at the SOTS site predeployment and postdeployment in March 2010, August 2011, July 2012, and May 2013. These observations are presented along with observations from RV *Aurora Australis* voyages in the SAZ in March 1998 and January 2007 (Figure 3). Discrete TCO_2 and TA were determined by coulometric and (open cell) potentiometric titration, respectively, following standard procedures [*Dickson et al.*, 2007] at the CSIRO Marine and Atmospheric Research Laboratory in Hobart. The precision and accuracy of the TCO_2 and TA measurements are on the order of ±3 µmol kg^{-1}.

2.2. Partitioning Changes in pCO_2 Across Physical and Biological Drivers

A linear relationship between salinity and alkalinity ($n = 115$, $r^2 = 0.92$, $p < 0.001$) was derived from observations at the SOTS site described above (Figure 3d) and used to compute hourly values of TA using the salinity data measured on the mooring. The relationship between TA and salinity is consistent with earlier observations from this region [*Metzl et al.*, 1999] and is assumed to be seasonally invariant. The pCO_2 and TA data were then used to compute the seasonal cycles of TCO_2, pH (on the seawater scale), and aragonite saturation state (Ω), using the CO_2Sys program [*Lewis and Wallace*, 1998], with the equilibrium

constants of *Mehrbach et al.* [1973] refit by *Dickson and Millero* [1987]. The calcium (Ca^{2+}) concentration was assumed conservative and calculated from salinity. We assumed seasonally constant values of phosphate and silicate in the CO_2 system computations, which introduces an uncertainty of less than 0.5 μmol kg^{-1} in the derived TCO_2 concentrations.

The air-sea exchange of CO_2 was computed with the following equation:

$$F = k\alpha\Delta pCO_2, \tag{1}$$

where F is the flux, k and α are the gas transfer velocity, and the coefficient of solubility [*Weiss*, 1974], respectively, and ΔpCO_2 is the gradient in CO_2 between the ocean and the atmosphere. The gas transfer velocity was computed from hourly wind measurements (described above) and the formulations of *Wanninkhof* [1992], *Nightingale et al.* [2000], and *Sweeney et al.* [2007]. We found a maximum difference in the computed flux due to the choice of gas transfer parameterization of ±3 mmol C m^{-2} d^{-1}, for values ranging from ~ −5 to 30 mmol C m^{-2} d^{-1}. The formulation of *Wanninkhof* [1992] was used in the computations described below, for comparison with other Southern Ocean sites [e.g., *Currie et al.*, 2009].

The changes in mixed layer TCO_2 concentration are affected by the following: air-sea CO_2 exchange, vertical diffusion across the base of the mixed layer, entrainment of water from below the mixed layer, horizontal advection, and transfer between inorganic and organic carbon pools through the biological processes of photosynthesis and remineralization. In the SAZ, the mean wind-stress curl favors downwelling [e.g., *T. Trull et al.*, 2001], and we thus ignore changes in mixed layer TCO_2 resulting from upwelling of CO_2-rich Circumpolar Deep Water, which have been shown to be important for surface TCO_2 in waters south of the Polar Front [*McNeil et al.*, 2001]. The SOTS site is located between the westward flowing inputs from the Tasman Sea, centered around 44°S [*Herraiz-Borreguero and Rintoul*, 2011], and the eastward flowing Antarctic Circumpolar Current, concentrated along the Subantarctic Front (SAF) near 51°S (Figure 1b) [*Rintoul and Trull*, 2001]. At the SOTS site, the surface flow is typically westward, with speeds generally less than 20 cm s^{-1}. East-west horizontal gradients in mixed layer pCO_2 in this region are small [*Metzl et al.*, 1999; *Takahashi et al.*, 2012], thus, for the moment, the impact of horizontal advection is ignored; this choice will be evaluated in more detail below. Our upper ocean (<400 m) observations suggest a conservative relationship between TA and salinity (Figure 2d), and we thus assume that carbonate mineral formation is negligible at the SOTS site. Changes in mixed layer TCO_2 are therefore attributed to combination of air-sea CO_2 exchange (ΔTCO_2^{gas}), vertical entrainment and diffusion (ΔTCO_2^{vert}), and biological processes (ΔTCO_2^{bio}). The gas exchange, and vertical entrainment and diffusion terms can be estimated directly from observations, allowing the biological component of changes in mixed layer TCO_2 to be estimated by difference:

$$\Delta TCO_2^{bio} = \Delta TCO_2^{obs} - \Delta TCO_2^{gas} - \Delta TCO_2^{vert}. \tag{2}$$

By using this residual method to partition observed changes in TCO_2 without explicitly determining the impact of horizontal advection, these lateral processes are included in the resulting ΔTCO_2^{bio} term.

The contribution from gas exchange was computed from the air-sea CO_2 fluxes, described above, and mixed layer depth (see Figure 4e). Entrainment was computed assuming that only periods of deepening introduce subsurface waters into the mixed layer [e.g., *Shadwick et al.*, 2011]. Vertical diffusion was computed following *Weeding and Trull* [2014], using a constant eddy diffusivity of 0.33×10^{-4} m^2 s^{-1} [*Law et al.*, 2003]. We applied a constant subsurface TCO_2 concentration of 2125 ± 10 μmol kg^{-1}, representative of SAMW, and the upper limit on the observed concentrations at the SOTS site over all seasons between 100 and 400 m depth (see Figure 3c). We used a linear gradient (over 50 m) between the subsurface and mixed layer value; observed profiles of TCO_2 from the SOTS site indicate that gradients occur over roughly this depth range directly below the mixed layer in all seasons (Figure 3c).

Using a similar approach as described for TCO_2, with the additional inclusion of temperature effects, the seasonal changes in pCO_2 were attributed to physical and biological drivers:

$$\Delta pCO_2^{obs} = \Delta pCO_2^{temp} + \Delta pCO_2^{gas} + \Delta pCO_2^{vert} + \Delta pCO_2^{bio}, \tag{3}$$

with superscripts of ΔpCO_2 corresponding to variations resulting from the changes in temperature (temp) and changes in TCO_2 (gas, vert, and bio). Each term in equation (3) was computed by assuming that the

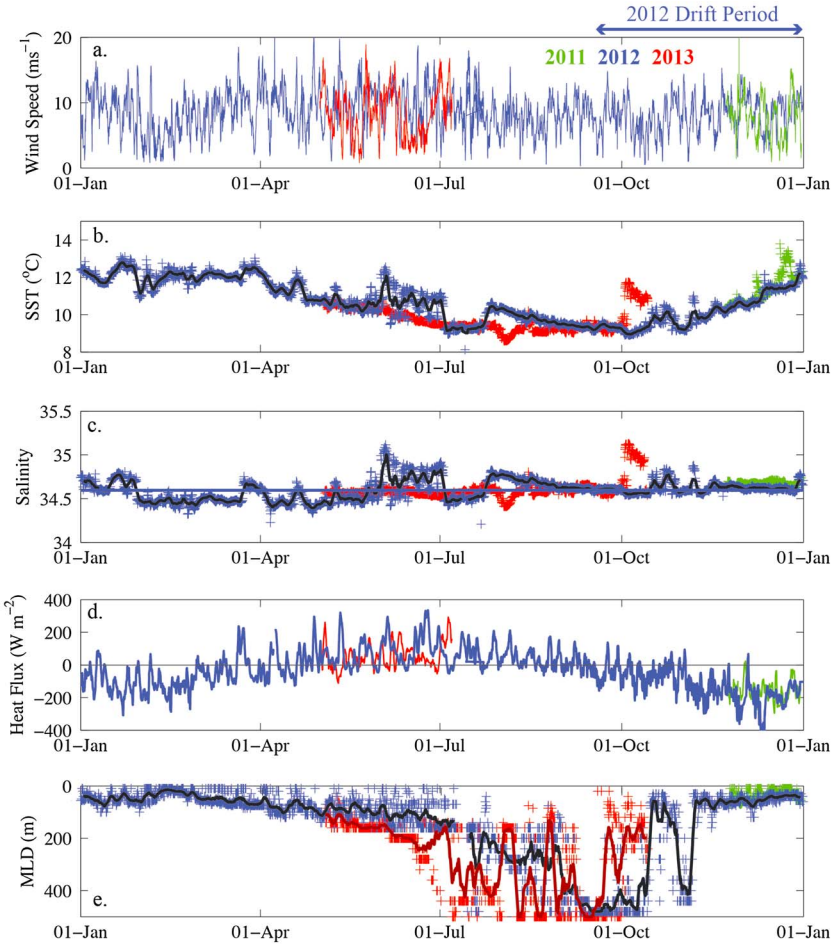

Figure 4. Atmospheric and hydrographic observations at the SOTS station: (a) wind speed, (b) sea surface temperature (SST), (c) sea surface salinity, (d) heat flux, and (e) mixed layer depth (MLD). In all panels observations from 2011, 2012, and 2013 are shown in green, blue, and red, respectively. The bold black lines in Figures 4b, 4c, and 4e, indicate daily averages of the 2012 data, and in Figure 4c, the bold blue line indicates the annual mean salinity (S_{mean} = 34.60) in 2012. The period of eastward drift (see Figure 1b) from 24 September to 31 December 2012 is indicated above Figure 4a.

process acted on the carbonate system individually; the changes in TCO_2 (and temperature) were considered in turn, while other variables were held constant [e.g., *Shadwick et al.*, 2011; *Jiang et al.*, 2013]. The difference in pCO_2 between the original (observed) and modified conditions were then computed.

To explore the impact of advective changes on TCO_2, and consequently pCO_2, anomalies in salinity and ΔpCO_2^{bio} were used. The salinity anomalies were defined as deviations greater than 0.05 from the annual mean (2012) salinity; the ΔpCO_2^{bio} anomalies were defined as deviations greater than 10 µatm from a (polynomial) model fit to the (computed) seasonal cycle.

Uncertainties associated with each of the terms in equation (2) were estimated and are summarized in Table 1. The pCO_2 uncertainty is associated with the measurement by the MAPCO2 system (see section 2.1). The uncertainty associated with TA concentrations was estimated from the residuals of the linear fit to the relationship between observed TA and salinity (Figure 3d). There is a relatively large uncertainty associated with TCO_2 resulting from the CO_2 system computations with TA and pCO_2 as input variables; the corresponding uncertainty associated with computed pH and Ω are 0.01 and 0.1, respectively. The uncertainty associated with TCO_2 concentration of the subsurface SAMW (for the vertical entrainment and diffusion terms) results from the seasonal variability observed in profiles at the SOTS site (Figure 2c). We applied a 30% uncertainty to the air-sea CO_2 flux term, largely due to the uncertainty in the parameterization of the gas transfer velocity (equation (1)), [see *Naegler et al.*, 2006; *Watson et al.*, 2009]. To estimate the uncertainty associated with the mixed layer depth, determined on the basis of temperature observations

Table 1. Uncertainty Associated With Terms Used in the Estimate of Annual NCP, Computed From ΔTCO_2^{bio}, See Equation (2)

Parameter	Uncertainty	Details
pCO_2 (µatm)	2	From MAPCO$_2$ system measurement
TA (µmol kg^{-1})	5	From fit to discrete observations of TA and salinity (Figure 2d)
TCO_2 (µmol kg^{-1})	11	From CO_2 system computations (with TA and pCO_2)
TCO_2^{SAMW} (µmol kg^{-1})	10	From range of subsurface TCO_2 observations (Figure 2c)
F (mmol C m^{-2} d^{-1})	2	From gas transfer parameterization
MLD (m)	22	Difference between values based on temperature and density
NCP (mmol C m^{-2} yr^{-1})	1.5 (~ 60%)	Propagation of above: $\sqrt{\sum(\text{errors}^2)}$

(see section 2.1), we computed mixed layer depth for the profiles at the SOTS site (Figure 3) using both temperature and density criteria. We found that the mean difference in mixed layer depth between the methods was less than 15%; we therefore assume a 15% uncertainty on our mixed layer depth computations using hourly temperature observations. These errors were propagated through the computation of ΔTCO_2^{bio} and the corresponding (annual) estimate of NCP (Table 1).

3. Results and Discussion

3.1. Seasonal Cycles

Atmospheric and hydrographic observations between 2010 and 2012 reveal expected annual evolutions of surface water properties [e.g., *Rintoul and Trull*, 2001; *T. Trull et al.*, 2001]: a seasonal temperature cycle with a magnitude of 4°C (from a minimum of ~8.5°C to a maximum of ~12.5°C); mixed layer depths increasing from a seasonal minimum of ~50 m to >400 m in the winter and spring; relatively constant salinity; and strong winds throughout the year (Figure 4). Observations from the three deployments reveal modest interannual variability in hydrographic properties, with similar seasonal cycles of temperature and salinity in 2011, 2012, and 2013. During the period when the mooring drifted eastward (see Figure 1b), surface water properties were consistent with observations at the SOTS site immediately before the drift period, and with observations from the same time of year in 2011 (Figure 4). We therefore treat the drift period as part of the 2012 annual record.

Short-term departures from mean salinity and temperature (Figures 4b and 4c) are observed in all years, lasting from days to several weeks. Unlike temperature and salinity, the seasonal evolution of mixed layer depth indicates significant interannual variability, with respect to the onset of deep mixing in autumn and shoaling in spring (Figure 4d). The impact of high-frequency hydrographic variability and the timing of seasonal changes in mixed layer depth on the carbon system is discussed in more detail below.

The magnitude of the seasonal cycle in surface water pCO_2 is on the order of 60 µatm, from a minimum of ~330 µatm in the summer, to near-atmospheric equilibrium (~390 µatm) in spring (September, see Figure 5a). In contrast, atmospheric pCO_2 varied by less than 5%. Almost all this variability was driven by total atmospheric pressure, and the atmospheric CO_2 mole fraction exhibits a very small seasonal variation, remaining nearly constant at a mean annual value of 390 ppm in 2012, with minimum and maximum values of 387.5 ppm and 391 ppm, respectively (Figure 5a). These values and associated weak seasonality are consistent with observations at the Cape Grim Remote Atmospheric Baseline station in northwestern Tasmania, where the annual average atmospheric CO_2 in 2012 was 390.0 ± 1.2 ppm (data available online at http://www.csiro.au/greenhouse-gases/).

The magnitude of the seasonal cycle of surface water pCO_2 and the degree of winter disequilibrium with the atmosphere (~ ±5 µatm) are consistent with earlier observations in the SAZ [*Metzl et al.*, 1999; *Takahashi et al.*, 2009]. The SOTS pCO_2 observations presented here indicate very similar seasonality to earlier observations, with concentrations approximately 40 µatm higher in 2012 relative to the observations (largely from the early 1990s) complied by *Metzl et al.* [1999]. This is broadly consistent with the increase in atmospheric CO_2 over this period (~36 µatm between 1992 and 2012), suggesting that surface waters in the SAZ are tracking the global ocean average response [e.g., *Takahashi et al.*, 2009]. Furthermore, observations from the SOTS site have a similar seasonality to the gridded data from *Takahashi et al.* [2012], which indicate

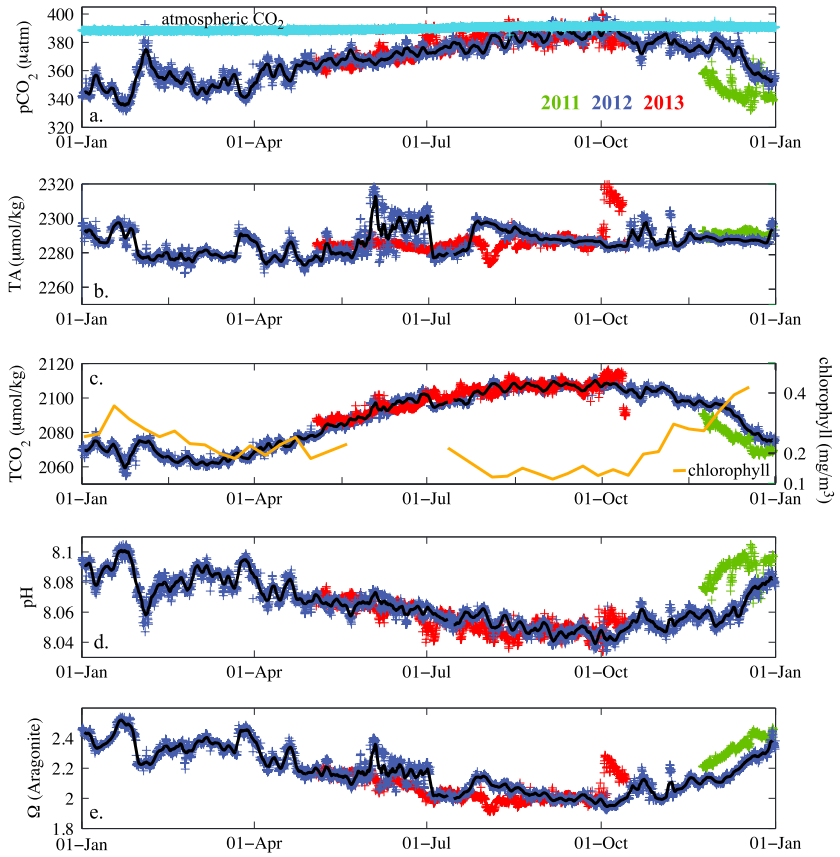

Figure 5. CO_2 system parameters at the SOTS station: (a) observed surface ocean pCO_2 and atmospheric CO_2 (pale blue line, mole fraction in dry air, in ppm); (b) computed total alkalinity (TA); (c) computed dissolved inorganic carbon (TCO_2) and satellite chlorophyll-a concentration (orange line); (d) computed pH; and (e) computed aragonite saturation state (Ω). In all panels observations from 2011, 2012, and 2013 are shown in green, blue, and red, respectively, and the bold black lines indicate daily averages of the 2012 data.

near-atmospheric equilibrium of the surface waters from a brief period in winter and seasonal range of roughly 30 µatm, with small zonal and larger north-south gradients.

Surface TA, computed as a function of salinity (see section 2, Figure 3d), indicates relatively constant values throughout the year, while the seasonality of TCO_2 indicates minimum concentrations of roughly 2060 µmol kg^{-1} in summer (coincident with annual minimum pCO_2), and maximum concentrations of greater than 2100 µmol kg^{-1} (coincident with maximum pCO_2), in spring. The annual evolution of both pH and aragonite saturation state (Ω) mirrors the seasonality in pCO_2, with annual maxima in winter and minima in spring (Figures 5d and 5e); the magnitude of the seasonal cycles in pH and Ω are roughly 0.06 and 0.34, respectively. The annual mean surface ocean pH at the SOTS site (8.07), is lower than the (zonally averaged) Southern Hemisphere high-latitude surface water mean (~8.13, based on GLODAP data; [*Key et al.*, 2004]), while the annual mean Ω (2.18) is somewhat higher than this mean value (~1.87) throughout the year.

3.2. Physical and Biological Controls of the CO_2 System

The thermal component of seasonal changes in pCO_2 ranges from a maximum of ΔpCO_2^{temp} = 30 µatm between late November and April, to a minimum of ΔpCO_2^{temp} = −30 µatm in July (Figure 6a). This seasonal change in pCO_2, driven by changes in surface temperature, is less than half the magnitude of the thermal component observed in the North Pacific and North Atlantic [e.g., *Takahashi et al.*, 2002] at similar latitudes, and due to the small amplitude seasonal temperature cycle in the SAZ (Figure 4b). Air-sea CO_2 fluxes ranged from 1 to 20 mmol C m^{-2} d^{-1}, with the largest fluxes observed between January and June, coincident with the largest air-sea CO_2 disequilibrium. The impact of this oceanic CO_2 uptake on surface pCO_2 was modest: $0.5 < \Delta pCO_2^{gas} \leq 6$ µatm.

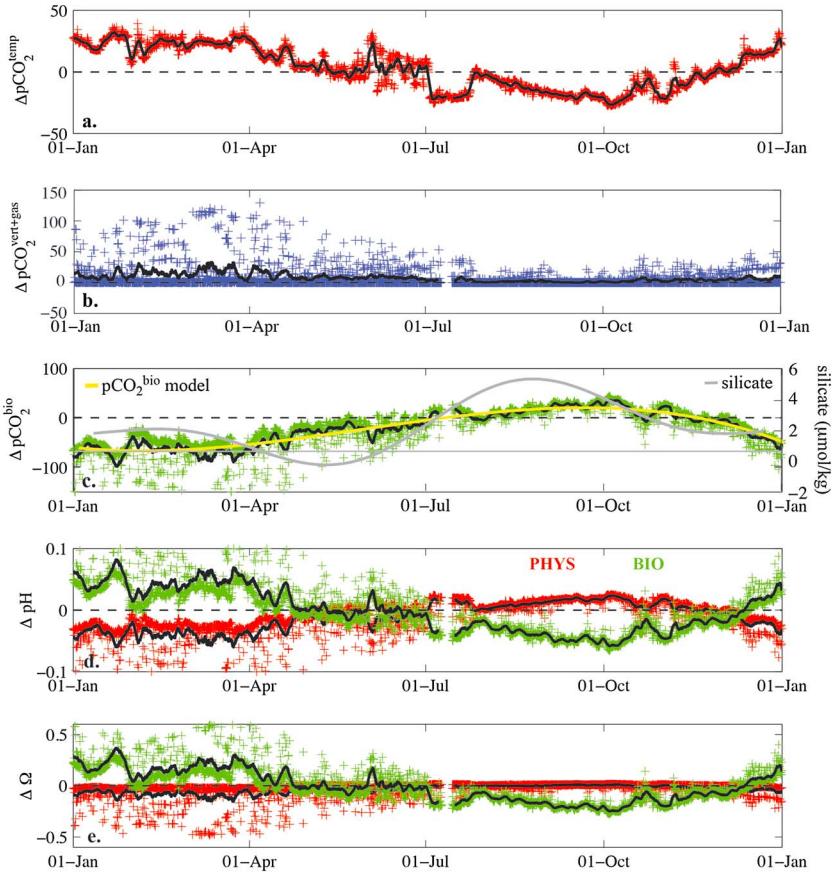

Figure 6. Partitioning across physical and biological controls on the CO_2 system at the SOTS station in 2012: (a) the temperature component of seasonal changes in pCO_2; (b) the combined influence of vertical entrainment and diffusion, and air-sea gas exchange on pCO_2; (c) the biological component of seasonal changes in pCO_2 (in green), with the polynomial fit to the seasonal cycle of ΔpCO_2^{bio} in yellow, the seasonal cycle in surface silicate (from the CARS Atlas) shown by the bold grey line, and the thin grey line indicating silicate concentrations equal to 1 μmol kg^{-1}; (d) the physical (temperature, vertical entrainment and diffusion, and gas exchange, shown in red) and biological (in green) contributions to seasonal changes in pH; and (e) as in Figure 6d but for Ω. The bold black lines represent daily averages of the data in all panels.

The supply of TCO_2-rich subsurface waters to the mixed layer by deep winter mixing plays an important role in controlling surface pCO_2 [*Metzl et al.*, 1999]. The seasonal observations presented here allow a high-frequency quantification of this vertical supply and the corresponding impact on surface pCO_2. We find that short-term (based on hourly observations) increases in pCO_2, of greater than 100 μatm, result from entrainment of subsurface waters (Figure 6b). By contrast, we find the contributions from vertical diffusion to be negligible (<2 μatm) throughout the year. However, given that entrainment is computed only during periods of mixed layer deepening, many of the hourly observations (during periods of mixed layer shoaling) return a null value; using a daily average, the ΔpCO_2^{vert} is between 5 and 30 μatm. The TCO_2 gradients between the surface and the water column below the mixed layer are largest in summer and early autumn, when mixed layer depths are less than 200 m (Figure 3c); the (daily) impact of entrainment (ΔpCO_2^{vert} = 20 to 30 μatm) is therefore dominant in these seasons because the volume of water through which the entrained signal is diluted is not that large. By contrast, in winter, when mixing extends to greater than 400 m, the gradient in TCO_2 between the surface and below the mixed layer is smaller (Figure 3c), and given the large volume of water in the mixed layer, the impact of entrainment (ΔpCO_2^{vert} ~10 μatm) is smaller than that observed in autumn. Thus, while the vertical supply of TCO_2-rich waters is important in controlling seasonal changes in surface pCO_2, the (maximum) magnitude of this process is similar to the thermal component. Furthermore, while these observations reinforce earlier studies which attribute the winter near atmospheric equilibrium of pCO_2 in the SAZ to deep mixing [*Metzl et al.*, 1999, 2006], our annual observations allow this

to be refined, identifying the period of autumn mixing, to depths less than 200 m as dominant over very deep winter mixing, with respect to subsurface contributions to surface pCO_2.

The biological component of seasonal changes in pCO_2 was estimated by difference after each of the physical drivers described above were quantified (Figure 6c). Our observations indicate a biologically driven decrease in pCO_2 over the productive season from December through June (described in more detail below) that ranged from $\Delta pCO_2^{bio} = -120$ to -20 µatm. Outside of the productive season (July to November), respiration or remineralization of organic matter increases pCO_2 by up to 40 µatm, with a corresponding increase of ~10 µmol kg^{-1} in ΔTCO_2^{bio} (not shown). The required pool of particulate and/or dissolved organic matter required to close the annual cycle by respiration, as suggested by our analysis, is on the order of 10–20 µmol kg^{-1}. Suspended particulate organic carbon (POC) concentrations of 4 ± 3 µmol kg^{-1} at the end of the summer period, representing less than half of this requirement have been reported [*Lourey and Trull*, 2001]. A late summer increase in dissolved organic carbon (DOC) on the order of 15–25 µmol kg^{-1}, which must later be mixed away or respired, has also been observed at the SOTS site (T. W. Trull and D. Davies, RV *Aurora Australis* Voyage AA9706, unpublished data, March 1998). Thus, there may be sufficient POC and/or DOC to fuel the estimated winter respiration in the region. This finding differs from earlier modeling studies that suggest a dominance of vertical supply in restoring winter nutrient concentrations at the SOTS site [*Wang et al.*, 2001]. However, because our estimated ΔpCO_2^{bio} includes potential contributions from horizontal advection (see section 2), the winter return to atmospheric equilibrium is likely due to a combination of respiration and horizontal inputs.

Because the ΔpCO_2^{bio} term is computed using hourly observations of changes in mixed layer depth (to quantify the physical drivers), which can be significant in the SAZ (Figure 4e), we resolve variations in the biological component that are likely too rapid to be representative of in situ processes. High-frequency observations of mixed layer depth are not often used in mixed layer mass balance approaches to partition changes in TCO_2 and pCO_2 since monthly or seasonal observations are more readily available, resulting in relatively smoothly varying, or climatological, annual cycles of mixed layer depth and drivers of changes in mixed layer TCO_2 and pCO_2 [e.g., *Gruber et al.*, 1998; *Shadwick et al.*, 2011; *Brix et al.*, 2013; *Jiang et al.*, 2013]. The impact of these high-frequency variations remains evident in the daily average of ΔpCO_2^{bio}, which is pulled away from the zero line in response to rapid increases in autotrophy in the first half of the year (Figure 6c), and which we consider to be representative of processes occurring in the surface layer. The impact of hydrographic changes acting on time scales of days to weeks on ΔpCO_2^{bio} will be explored in more detail (section 3.4).

The combined physical (temperature, vertical entrainment and diffusion, and gas exchange) and biological controls on seasonal changes in pH and Ω are similar to those described above for pCO_2 (Figures 6d and 6e). Warming (from November to July), vertical supply of TCO_2-rich water, oceanic CO_2 uptake, and respiration all act to decrease pH. During the productive season, biologically driven increases in pH are of equal magnitude to the (combined) physically driven decreases. From July to December, cooling (which increases pH) and a reduced supply of water from below allow heterotrophic decreases in pH to outweigh the physically driven increases. The seasonality in Ω is somewhat different than that of pH due to the opposing effect of temperature; warming from December to July results in modest increases in Ω, such that the biological control on the seasonal cycle is larger than the physical control throughout the year. Understanding the subtle differences in the seasonality of physical and biological drivers on pH and Ω is important to predicting the evolution of high-latitude systems to anthropogenic change [*Shadwick et al.*, 2013]. In the SAZ south of Australia, the southward extension of the (warm) East Australian Current [e.g., *Cai et al.*, 2005; *Ridgway*, 2007] will amplify the effects of ocean CO_2 uptake on pH while partially countering the associated decrease in Ω.

3.3. Net Community Production and Initiation of Springtime Production

The annual cycle of ΔpCO_2^{bio} indicates a clear delineation between the autotrophic season, when production exceeds respiration ($\Delta pCO_2^{bio} < 0$), and the heterotrophic season, when respiration dominates ($\Delta pCO_2^{bio} > 0$, Figure 6c). From the seasonal evolution of ΔTCO_2^{bio} (not shown), we estimate an annual net community production (NCP, the imbalance between net primary production and heterotrophic respiration) of 2.45 ± 1.47 mol C m^{-2} yr^{-1} (~29 g C m^{-2} yr^{-1}), at the SOTS site. The export fluxes of particulate organic carbon at 1000 m, 2000 m, and 3900 m, at this location between August 2011 and July 2012 were 1.9, 1.6, and 1.1 g C m^{-2} yr^{-1}, respectively (S. Bray, personal communication, 2014) and consistent with earlier

observations [*T. W. Trull et al.*, 2001]. Our computed NCP represents an upper limit on the amount of material available for export to the subsurface; in 2012, the flux at 1000 m represents roughly 7% of the surface production.

Our (annual) NCP is somewhat larger than the estimate of *Weeding and Trull* [2014], who reported 1.57 ± 0.85 mol C m^{-2} yr^{-1}, based on an oxygen budget in the mixed layer at the SOTS site and converted to carbon units by scaling by 1.4 [e.g., *Laws*, 1991; *Bender et al.*, 1999], though in the same range when the uncertainties are taken into account. The *Weeding and Trull* [2014] estimate used observations between September 2010 and April 2011 and thus covers only part of the annual record in a different year. Interestingly, their observations, as well as the 2011 pCO_2 observations shown in Figure 4a suggest that biological production was underway in September, i.e., early spring, and ceased in December, or early summer. The seasonal cycle of ΔpCO_2^{bio} presented here indicates that in 2012 autotrophy continued through the autumn, with net production ceasing in June and the subsequent autotrophic season commencing in early December, indicating that interannual variability in the timing of the onset of production may be significant at this location.

In late 2012 we observe a decrease in pCO_2 (and $\Delta pCO_2^{bio} < 0$), near the beginning of October, coincident with a short-term shoaling of the mixed layer from greater than 400 m to roughly 100 m (Figure 4e). This period of shoaling is followed by an episode of deep mixing, to roughly 400 m, a coincident increase in pCO_2 to near-atmospheric equilibrium, and values of $\Delta pCO_2^{bio} > 0$. When stratification is achieved in early November, we see a sustained decrease in pCO_2 and a maintenance of $\Delta pCO_2^{bio} < 0$, indicating net autotrophic conditions and the onset of the spring bloom. Additionally, the initial October decrease in pCO_2, as well as the sustained decrease in November are broadly consistent with increases in surface chlorophyll concentration, inferred from the 8 day MOIDIS satellite data (Figure 5c). Our observations indicate a reversal in the sign of the heat flux that corresponds to the onset of prolonged stratification in November, supporting the notion that the shutdown of convection may serve as an indicator of bloom initiation [*Taylor and Ferrari*, 2011]. The 2013 data indicate that the mixed layer remained quite deep (~200 m) in early October, and corresponding pCO_2 values near-atmospheric equilibrium suggest that the initiation of net production may have been delayed until the onset of stratification (i.e., a view consistent with the concept of a critical stratification depth; [*Sverdrup*, 1953]).

3.4. Salinity and ΔpCO_2^{bio} Anomalies

The resolution of hydrographic and pCO_2 observations at the SOTS site allow detailed examination of high-frequency events, lasting between several days and several weeks. We defined salinity and ΔpCO_2^{bio} anomalies (see section 2, Figures 7a and 7b) and here explore the relationship between the two, effectively allowing the impact of grouping horizontal advection and biology together in the partitioning of changes in pCO_2 to be evaluated.

We observed events, i.e., coincident salinity and ΔpCO_2^{bio} anomalies, falling into three broad categories: (1) fresh with weakening of the biological pump; (2) saline with strengthening of the biological pump; and (3) fresh with strengthening of the biological pump (Figure 7c). The majority of events fall into the first category, where surface waters are fresher than the annual mean salinity, and the biological pump is weakened, reflected by a positive ΔpCO_2^{bio} anomaly. These events were observed throughout the year, in both the autotrophic and heterotrophic periods (Figure 6a). For example, at the end of January (at the height of the autotrophic season), when surface pCO_2 is near the annual minimum (Figure 5a), we observed a freshening of the surface waters, associated with a positive ΔpCO_2^{bio} anomaly, indicating a weakening of the biological pump. This freshening event was also associated with a decrease in TA and an increase in observed pCO_2 from the seasonal minimum (~330 µatm) to ~370 µatm over a period roughly 10 days (event E1, in Figure 7). Another event in this first category (freshening and weakening of the biological pump) was observed near the beginning of the heterotrophic period in mid-July (event E4 in Figure 7). In this case the freshening event was associated with decreased TA and decreased pCO_2, corresponding to a dampening of the net heterotrophic signal and a positive ΔpCO_2^{bio} anomaly, that persisted for less than 10 days.

In the second most common class of events, surface waters are more saline than the annual mean, and the biological pump is strengthened. These events were also observed throughout the year, regardless of the net autotrophic or heterotrophic status of the surface waters. We observed a relatively long-lived saline anomaly, from early June through early July (in the autotrophic period), with a coincident enhancement of TA (see Figure 5b). This event (E3 in Figure 7) is associated with a modest decrease in observed pCO_2, smaller

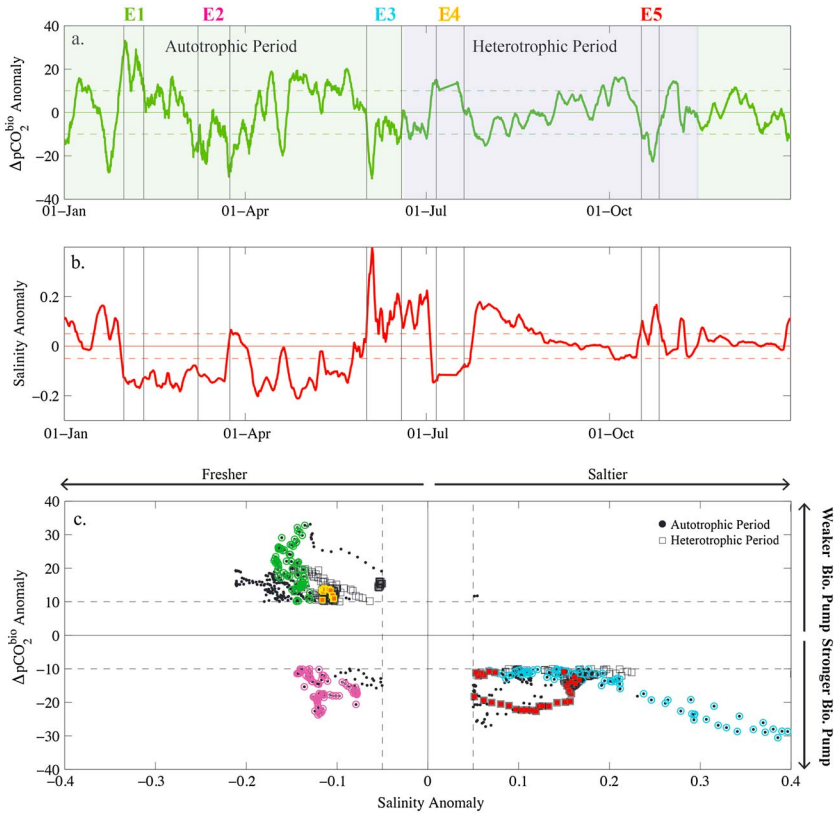

Figure 7. The impact of the advection of high- and low-salinity waters on the biologically driven changes in surface pCO_2: (a) ΔpCO_2^{bio} anomalies with the auto/heterotrophic period indicated by the green/blue shading; (b) salinity anomalies; and (c) the relationship between ΔpCO_2^{bio} anomalies and salinity anomalies, with the autotrophic (black circles) and heterotrophic (black squares) periods of the season indicated. Five events (E1 to E5, described in section 3.4) are indicated above Figure 7a and are plotted according to the text color with circles (autotrophic period) or squares (heterotrophic period) in Figure 7c).

than what might be expected from the roughly 20 μmol kg^{-1} increase in TA and a strengthening of the biological pump (a negative ΔpCO_2^{bio}), particularly at the beginning of the event, when the largest change in salinity is observed. A shorter event of the same type was observed toward the end of the heterotrophic period, over roughly 10 days in mid-October (event E5 in Figure 7), in which the positive salinity anomaly was associated with a strengthening of the biological pump (a negative ΔpCO_2^{bio} anomaly), an increase in TA, and decrease in surface pCO_2 (see Figures 5a and 5b).

Previous studies in the SAZ have shown that biomass is higher in the north and starts earlier in the season; the waters in the northern region, closer to the Subtropical Front (STF), are also more saline (and warmer, Figure 1b; [*Bowie et al.*, 2011]). Thus, the saline events likely reflect the input of water from the north, which bring biomass, either as particles or their imprint on the surface TCO_2 field, enhancing autotrophy during the productive season and fuelling additional heterotrophy outside of the productive period. The fresh events, which are likely the result of inputs of water from the south do not supply "additional" biomass and thus weaken the biological pump in both the productive and heterotrophic periods. Another parallel view of these processes is that the fresh/salty, weaker/stronger biological pump events reflect the influence of the far-field surface TCO_2; a maximum (surface) concentration gradient of 30 μmol kg^{-1} in TCO_2 is required to produce the ΔpCO_2^{bio} anomaly of 60 μatm (i.e., ±30 μatm). Based on TCO_2 observations from the WOCE SR3 section (see Figure 1), mixed layer TCO_2 varies from 2085 μmol kg^{-1} at 46°S to 2100 μmol kg^{-1}48.5°S, indicating that north-south gradients (with surface TCO_2 increasing southward) large enough to explain the ΔpCO_2^{bio} anomalies are present over a relatively small spatial range in the SAZ. The duration of the events may also suggest the influence of eddies in changing surface properties; mesoscale motions in the region are common [e.g., *Weeding and Trull*, 2014] and north-south gradients in surface

temperature (see Figure 1b) and salinity are large enough to explain the observed salinity anomalies at the SOTS site [e.g., *Lourey and Trull*, 2001].

The third class of events, characterized by surface waters fresher than the annual mean, and a strengthening of the biological pump, are only observed in the summer season, and under net autotrophic conditions (Figure 7). The origin of these events is unknown, but the relief of either silicic acid or iron limitation is a possible explanation. The SAZ region undergoes seasonal depletion of silicic acid when nitrate remains available; based on the 2007 SAZ-Sense study [*Bowie et al.*, 2011] and climatological concentrations from CARS (see section 2; [*Ridgway et al.*, 2002]), silicic acid is limiting well before the end of the autotrophic period (<1 μmol kg^{-1}, Figure 6c). Given that these fresh anomalies likely originate in the south, they may also supply silica to the extent that they bring macronutrient rich water northward across the Subantarctic Front [*Rintoul and Trull*, 2001]. We observe short-term (on the order of 10 days) freshening events associated with negative ΔpCO_2^{bio} anomalies only in late March and early April (event E2, for example, in Figure 7), consistent with the onset of silica limitation and suggesting a stimulation of biological production associated with pulses of fresh water. Relief of iron limitation by aerosol inputs, potentially associated with freshening by wet deposition, is also a possibility given that surface iron enrichments have been observed in spring and summer [*Sedwick et al.*, 1997, 2008; *Lannuzel et al.*, 2011].

3.5. Comparison With Other High-Latitude Observations

Time series observations of physical and biogeochemical variables at the seasonal and subseasonal time scale have done much to resolve uncertainties in carbon cycling at a few important study sites (e.g., Bermuda, Hawaii; [*Bates et al.*, 1995; *Karl and Lukas*, 1996]), though the majority of these efforts have been restricted to the Northern Hemisphere [*Bates et al.*, 2014]. An exception is the routine sampling of waters at the STF east of New Zealand (Munida Station, [*Currie et al.*, 2009]), which provides a unique subantarctic parallel to our observations at the SOTS site.

The (median) annual amplitude of pCO_2 at the Munida Station (between 1998 and 2009) is on the order of 30 μatm [*Brix et al.*, 2013], which is roughly half the magnitude of that observed at the SOTS site. This discrepancy may be due in part to the sparser (bimonthly) temporal resolution of the Munida pCO_2 observations; the January 2012 pCO_2 minima we observed at the SOTS site was short-lived (Figure 5a), and followed by a rapid increase of roughly 50 μatm, associated with a freshening event (E1, described in the previous section) lasting less than 2 weeks, a feature that would not necessarily have been captured with bimonthly sampling. Daily rates of summer NCP at the Munida station, based on observations of pCO_2 and TA and a one-dimensional model for mixed layer TCO_2, are roughly 20 mmol C m^{-2} d^{-1} (based on a drawdown of ~33 μmol kg^{-1} over 90 days of summer and an average mixed layer depth of ~55 m; [*Brix et al.*, 2013]). From the computed annual cycle of ΔTCO_2^{bio} (see equation (2)), similar daily rates of NCP (~20 mmol C m^{-2} d^{-1}) from mid-October to the end of the year at the SOTS site are estimated from a 30 μmol kg^{-1} decrease in TCO_2^{bio} over 2.5 months. Our analysis indicates that the productive season in the SAZ proceeds slowly from its initiation in mid-October, coincident with mixed layer shoaling (see section 3.3), to its cessation in late June (Figure 6c). Observations at both the Munida Station and the SOTS site indicate that biological carbon uptake exerts a dominant control on surface water pCO_2 and correspondingly on the uptake of atmospheric CO_2 in these regions of the SAZ.

The SAZ is characterized by high-nutrient, low-chlorophyll (HNLC) conditions, which extend, broadly speaking, in a zonally homogeneous ring around the globe. These HNLC surface waters are not associated with an annual phytoplankton bloom, a phenomenon which occurs annually in the North Atlantic Ocean [e.g., *Siegel et al.*, 2002]. Daily rates of primary production in the North Atlantic (at 47°N, a similar northern latitude to the SOTS site), based on both the ^{14}C assimilation method and observations of TCO_2, of 84 to 107 mmol C m^{-2} d^{-1} over a 12 day period have been reported [*Chipman et al.*, 1993]. These observations are comparable to the rapid decreases in pCO_2, from >400 to ~250 μatm, and TCO_2 (from 2060 to 1980 μmol kg^{-1}) observed over 2 weeks in the Scotian Shelf region of the northwestern Atlantic [*Shadwick et al.*, 2010, 2011]. By contrast, the seasonal decrease in pCO_2 of roughly 60 μatm (and daily rates of NCP smaller by a factor of 4 to 5) at the SOTS site occurs over a period of several months in the absence of rapid increases in biomass observed annually at similar latitudes in the North Atlantic.

Parallels are routinely drawn between the seasonally silicate-depleted HNLC waters of the subarctic North Pacific [e.g., *Wong and Matear*, 1999] and the SAZ, often as a result of a lack of observations from the latter system [e.g., *Banse*, 1996]. The annual cycle of pCO_2 from Ocean Station Papa (OSP, 50.12°N, 144.83°W;

http://cdiac.ornl.gov/oceans/time_series_moorings.html) in the eastern subarctic North Pacific indicates a seasonal magnitude of <30 μatm in surface pCO_2 (based on observations from June 2010 to June 2011), roughly half that observed at the SOTS site (Figure 5a). The magnitude of the seasonal temperature cycle is, however, much larger (~10°C at OSP compared to ~4°C at SOTS), and the seasonal warming counteracts the biologically mediated pCO_2 decrease during the summer season, maintaining surface pCO_2 closer to atmospheric equilibrium than at the SOTS site. By contrast, in the western subarctic North Pacific at station K2 (47°N, 160°E, [*Honda et al.*, 2006]), the magnitude of the seasonal cycle in surface pCO_2 is ~100 μatm (based on more than a decade of observations between 1992 and 2008), with late winter/early spring supersaturation of the surface waters [*Wakita et al.*, 2010]. Like OSP in the eastern North Pacific, K2 undergoes significant warming (~15°C) coincident with the seasonal depletion in TCO_2, and opposing the biologically mediated decrease in pCO_2 [*Wakita et al.*, 2010]. Differences in seasonal cycles of inorganic carbon and nutrients in the western and eastern subarctic North Pacific have been reported [*Harrison et al.*, 2004]. It is clear from observations at the SOTS site that the smaller seasonal warming and the prolonged biological pCO_2 drawdown in the SAZ drive seasonality that differs from both western and eastern HNLC subarctic North Pacific cycles, and that results in a net annual uptake of atmospheric CO_2 in this region.

4. Conclusion

Autonomous, high-resolution measurements of surface water pCO_2 at an open ocean site in the Subantarctic Zone, covering a full annual cycle allowed seasonality in the physical and biological controls on the surface CO_2 system to be resolved. The biological control on pCO_2 during the productive season was up to 4 times larger than the thermal control. Entrainment of subsurface waters was dominant in early autumn in mixed layers of ~200 m, with the return to near-atmospheric equilibrium occurring in late winter and early spring due to heterotrophic increases in pCO_2. Physics and biology contributed equally to seasonal changes in pH, while biological processes dominated changes in carbonate saturation state. Changes in surface salinity acting on subseasonal time scales influenced pCO_2 throughout the year via the meridional advection of waters with different TCO_2 signatures. This region of the SAZ acts as a net annual sink for atmospheric CO_2 largely due to the summer time biology (that persists over several months), a small seasonal warming, and a relatively slow return to near equilibrium with the atmosphere that is achieved shortly before the onset of production in the subsequent season. These perspectives and the high-resolution observations of the CO_2 system will be useful in improving Southern Ocean carbon cycle models, which currently display a wide range of seasonal cycles.

Acknowledgments

This work was supported by the Australian Government's Cooperative Research Centres Program, through the Antarctic Climate and Ecosystems Cooperative Research Centre (ACE CRC). The SOTS moorings are supported by IMOS, the ACE CRC, and the Australian Marine National Facility. Mooring construction was carried out by Danny Mclaughlan, Jim La Duke, and David Cherry (all CSIRO). Mark Rosenberg (ACE CRC) led the mooring deployments and recoveries, with additional assistance by Stephen Bray (ACE CRC). Peter Jansen (IMOS) carried out preparation, installation, and data recovery from the CTD and temperature instruments. Predeployment and postdeployment instrument calibrations were carried out by Rob Key (CSIRO) for temperature and salinity. We thank Kate Berry for TCO_2 and TA analyses, Ben Weeding for mixed layer depth computations, and Andrew Lenton for providing the CARS data. We are grateful to Philip Boyd and Richard Matear for helpful discussions, and to two anonymous reviewers for thoughtful suggestions. Ocean color and sea surface temperature visualizations used in this study were produced with the Giovanni online data system, developed and maintained by the NASA GES DISC. The SOFS pCO_2 data are archived at the Carbon Dioxide Information Analysis Center (http://cdiac.ornl.gov/oceans/ime_series_moorings.html), hydrographic and meteorological data are archived at the Australian Integrated Marine Observing Network portal (http://www.imos.org.au/sots.html). This paper is contribution 3415 of the Virginia Institute of Marine Science, College of William and Mary.

References

Acker, J. G., and G. Leptoukh (2007), Online analysis enhances use of NASA Earth science data, *EOS Trans. AGU*, *88*, 14–17.

Banse, K. (1996), Low seasonality of low concentrations of surface chlorophyll in the Subantarctic water ring: Underwater irradiance, iron, or grazing?, *Prog. Oceanogr.*, *37*, 241–291.

Bates, N. R., A. F. Michaels, and A. H. Knap (1995), Seasonal and interannual variability of oceanic carbon dioxide species at the U.S. JGOFS Bermuda Atlantic Time-series Study (BATS) site, *Deep Sea Res., II*, *43*, 347–383.

Bates, N. R., Y. M. Astor, M. J. Church, K. Currie, J. E. Dore, M. González-Dávila, L. Lorenzoni, F. Muller-Karger, J. Olafsson, and J. M. Santana–Casiano (2014), A time-series view of changing ocean chemistry due to ocean uptake of anthropogenic CO_2 and ocean acidification, *Oceanography*, *27*, 126–141, doi:10.5670/oceanog.2014.16.

Bender, M., J. Orchardo, M.-L. Dickson, R. Barber, and S. Lindley (1999), In vitro O_2 fluxes compared with ^{14}C production at other rate terms during the JGOFS Equatorial Pacific experiment, *Deep Sea Res., I*, *46*, 637–654.

Bowie, A. R., D. Lannuzel, T. A. Remenyi, T. Wagener, P. J. Lam, P. W. Boyd, C. Guieu, A. T. Townsend, and T. W. Trull (2009), Biogeochemical iron budgets of the Southern Ocean south of Australia: Decoupling of iron and nutrient cycles in the subantarctic zone by the summertime supply, *Global Biogeochem. Cycles*, *23*, GB4034, doi:10.1029/2009GB003500.

Bowie, A. R., F. B. Griffiths, F. Dehairs, and T. W. Trull (2011), Oceanography of the subantarctic and Polar Frontal Zones south of Australia during summer: Setting for the SAZ-Sense study, *Deep Sea Res., II*, *58*, 2059–2070.

Brix, H., K. I. Currie, and S. E. M. Fletcher (2013), Seasonal variability of the carbon cycle in subantarctic surface water in the South West Pacific, *Global Biogeochem. Cycles*, *27*, 200–211, doi:10.1002/gbc.20023.

Cai, W., G. Shi, T. Cowan, D. Bi, and J. Ribbe (2005), The response of the southern annular mode, the East Australian Current, and the southern mid-latitude ocean circulation to global warming, *Geophys. Res. Lett.*, *32*, L23706, doi:10.1029/2005GL024701.

Chipman, D. W., J. Marra, and T. Takahashi (1993), Primary production at 47°N and 20°W in the North Atlantic Ocean: A comparison between the ^{14}C incubation method and the mixed layer carbon budget, *Deep Sea Res., II*, *40*, 151–169.

Currie, K. I., M. R. Reid, and K. A. Hunter (2009), Interannual variability of carbon dioxide drawdown by subantarctic surface waters near New Zealand, *Biogeochemistry*, *107*, 23–34, doi:10.1007/s10533-009-9355-3.

Dickson, A. G., and F. J. Millero (1987), A comparison of the equilibrium constants for the dissociation of carbonic acid in seawater media, *Deep Sea Res., II*, *34*, 1733–1743.

Dickson, A. G., C. L. Sabine, and J. R. Christian (Eds.) (2007), *Guide to Best Practices for Ocean CO_2 Measurement*, PICES Special Publication 3, North Pacific Marine Science Organization, Sidney, Canada.

Gruber, N., C. D. Keeling, and T. F. Stocker (1998), Carbon-13 constraints on the seasonal inorganic carbon budget at the BATS site in the northwestern Sargasso Sea, *Deep Sea Res., I*, *45*, 673–717.
Gruber, N., et al. (2009), Oceanic sources, sinks, and transport of atmospheric CO_2, *Global Biogeochem. Cycles*, *23*, GB1005, doi:10.1029/2008GB003349.
Harrison, P. J., F. A. Whitney, A. Tsuda, H. Saito, and K. Todokoro (2004), Nutrient and plankton dynamics in the NE and NW gyres of the Subarctic Pacific Ocean, *J. Oceanogr.*, *60*, 93–117.
Herraiz-Borreguero, L., and S. R. Rintoul (2011), Regional circulation and its impact on upper ocean variability south of Tasmania (Australia), *Deep Sea Res., II*, *58*, 2071–2081.
Honda, M. C., H. Kawakami, K. Sasaoka, S. Watanabe, and T. Dickey (2006), Quick transport of primary produced organic carbon to the ocean interior, *Geophys. Res. Lett.*, *33*, L16603, doi:10.1029/2006GL026466.
Jiang, Z.-P., D. J. Hydes, T. Tyrrell, S. E. Hartman, M. C. Hartman, C. Dumousseaud, Z. A. Padin, I. Skjelvan, and C. González-Pola (2013), Key controls on the seasonal and interannual variations of the carbonate system and air-sea CO_2 flux in the Northeast Atlantic (Bay of Biscay), *J. Geophys. Res. Oceans*, *118*, 785–800, doi:10.1002/jgrc.20087.
Karl, D. M., and R. Lukas (1996), The Hawaii Ocean Time-series (HOT) program: Background, rationale and field implementation, *Deep Sea Res., II*, *43*, 129–156.
Key, R. M., A. Kozyr, C. L. Sabine, K. Lee, R. Wanninkhof, J. L. Bullister, R. A. Feely, F. J. Millero, C. Mordy, and T.-H. Peng (2004), A global ocean carbon climatology: Results from Global Data Analysis Project (GLODAP), *Global Biogeochem. Cycles*, *18*, GB4031, doi:10.1029/2004GB002247.
Khatiwala, S., et al. (2013), Global ocean storage of anthropogenic carbon, *Biogeosciences*, *10*, 2169–2191.
Lannuzel, D., A. R. Bowie, P. Lam, A. Townsend, E. Ibisanmi, E. Butler, T. Wagener, and V. Schoemann (2011), Distribution of dissolved and particulate iron in the sub-Antarctic and Polar Frontal Southern Ocean (Australian sector), *Deep Sea Res., II*, *58*, 2094–2112.
Law, C., E. Abraham, A. Watson, and M. Liddicoat (2003), Vertical eddy diffusion and nutrient supply to the surface mixed layer of the Antarctic Circumpolar Current, *J. Geophys. Res.*, *108*(C8), 3272, doi:10.1029/2002JC001604.
Laws, E. A. (1991), Photosynthetic quotients, new production and net community production in the open ocean, *Deep Sea Res.*, *38*, 143–167.
Lenton, A., R. J. Matear, and B. Tilbrook (2006), Design of an observational strategy for quantifying the Southern Ocean uptake of CO_2, *Global Biogeochem. Cycles*, *20*, GB4010, doi:10.1029/2005GB002620.
Lenton, A., N. Metzl, T. Takahashi, M. Kuchinke, R. J. Matear, T. Roy, S. C. Sutherland, C. Sweeney, and B. Tilbrook (2012), The observed evolution of oceanic pCO_2 and its drivers over the last two decades, *Global Biogeochem. Cycles*, *26*, GB2021, doi:10.1029/2011GB004095.
Lenton, A., et al. (2013), Sea-air CO_2 fluxes in the Southern Ocean for the period 1990–2009, *Biogeosciences*, *10*, 4037–4054, doi:10.5194/bg-10-4037-2013.
Lewis, E., and D. W. R. Wallace (1998), *Program Developed for CO_2 Systems Calculations, ORNL/CDIAC 105*, Carbon Dioxide Information Analysis Center, Oak Ridge Natl. Lab., U.S. Dep. of Energy, Oak Ridge, Tenn.
Lourey, M. J., and T. W. Trull (2001), Seasonal nutrient depletion and carbon export in the Subantarctic and Polar Frontal Zones of the Southern Ocean south of Australia, *J. Geophys. Res.*, *106*, 31,463–31,487.
Lovenduski, N. S., N. Gruber, and S. C. Doney (2009), Toward a mechanistic understanding of the decadal trends in the Southern Ocean carbon sink, *Global Biogeochem. Cycles*, *22*, GB1017, doi:10.1029/2007GB003139.
McNeil, B. I., and B. Tilbrook (2009), A seasonal carbon budget for the sub-Antarctic Ocean, South of Australia, *Mar. Chem.*, *115*, 196–210.
McNeil, B. I., B. Tilbrook, and R. J. Matear (2001), Accumulation and uptake of anthropogenic CO_2 in the Southern Ocean, south of Australia between 1968 and 1996, *J. Geophys. Res.*, *106*, 31,431–31,445.
Mehrbach, C., C. H. Culberson, J. E. Hawley, and R. M. Pytkowicz (1973), Measurement of the apparent dissociation constants of carbonic acid in seawater at atmospheric pressure, *Limnol. Oceanogr.*, *18*, 897–907.
Metzl, N., B. Tilbrook, and A. Poisson (1999), The annual fCO_2 cycle and the air-sea CO_2 flux in the sub-Antarctic Ocean, *Tellus B*, *51*, 849–861.
Metzl, N., C. Brunet, A. Jabaud-Jan, A. Poisson, and B. Schauer (2006), Summer and winter air-sea CO_2 fluxes in the Southern Ocean, *Deep Sea Res., I*, *53*, 1548–1653.
Naegler, T., P. Ciais, K. Rodgers, and I. Levin (2006), Excess radiocarbon constraints on air-sea gas exchange and the uptake of CO_2 by the oceans, *Geophys. Res. Lett.*, *33*, L11802, doi:10.1029/2005GL025408L.
Nightingale, P. D., P. S. Liss, and P. Schlosser (2000), Measurements of air-sea gas transfer during an open ocean algal bloom, *Geophys. Res. Lett.*, *27*, 2117–2120.
Orsi, A. H., T. Whitworth, and W. D. Nowlin (1995), On the meridional extent and fronts of the Antarctic Circumpolar Current, *Deep Sea Res., I*, *42*, 641–673.
Pender, L., T. Trull, D. McLaughlin, and T. Lynch (2010), Pulse-A mooring for mixed layer measurements in the open ocean and extreme weather, Commonwealth Scientific and Industrial Research Organisation Marine and Atmospheric Research, paper presented at IEEE OCEANS Conference, Sydney, Australia.
Resplandy, L., J. Boutin, and L. Merlivat (2014), Observed small spatial scale and seasonal variability of the CO_2 system in the Southern Ocean, *Biogeosciences*, *11*, 75–90.
Ridgway, K. R. (2007), Long-term trend and decadal variability of the southward penetration of the East Australian Current, *Geophys. Res. Lett.*, *34*, L13613, doi:10.1029/GL030393.
Ridgway, K. R., J. R. Dunn, and J. L. Wilkin (2002), Ocean interpolation by four-dimensional least squares—Application to the waters around Australia, *J. Atmos. Oceanic Technol.*, *19*, 1357–1375.
Rintoul, S. R., and T. W. Trull (2001), Seasonal evolution of the mixed layer in the Subantarctic Zone south of Australia, *J. Geophys. Res.*, *106*, 31,447–31,462.
Sabine, C. L., et al. (2004), The Oceanic sink for anthropogenic CO_2, *Science*, *305*, 367–371.
Sallée, J.-B., R. J. Matear, S. R. Rintoul, and A. Lenton (2012), Localized subduction of anthropogenic carbon dioxide in the Southern Hemisphere oceans, *Nat. Geosci.*, *5*, 579–584, doi:10.1038/NGEO1523.
Sarmiento, J. L., N. Gruber, M. A. Brzezinski, and J. P. Dunner (2004), High-latitude control of thermocline nutrients and low latitude biological productivity, *Nature*, *427*, 56–60.
Schulz, E., S. A. Josey, and R. Verein (2012), First air-sea flux mooring measurements in the Southern Ocean, *Geophys. Res. Lett.*, *39*, LI6606, doi:10.1029/2012GL052290.
Sedwick, P. N., P. R. Edwards, D. J. Mackey, F. B. Griffiths, and J. S. Parslow (1997), Iron and manganese in surface waters of the Australian Subantarctic region, *Deep Sea Res., I*, *44*, 1239–1253.

Sedwick, P. N., G. R. DiTullio, D. A. Hutchins, P. W. Boyd, F. B. Griffiths, A. C. Crossley, T. W. Trull, and B. Queguiner (1999), Limitation of algal growth by iron deficiency in the Australian Subantarctic region, *Geophys. Res. Lett.*, *26*, 2865–2868.

Sedwick, P. N., A. R. Bowie, and T. W. Trull (2008), Dissolved iron in the Australian sector of the Southern Ocean (CLIVAR SR3 section): Meriodional and seasonal trends, *Deep Sea Res., I*, *55*, 911–925.

Shadwick, E. H., H. Thomas, A. Comeau, S. E. Craig, C. W. Hunt, and J. E. Salisbury (2010), Air-sea CO_2 fluxes on the Scotian Shelf: Seasonal to multi-annual variability, *Biogeosciences*, *7*, 3851–3867.

Shadwick, E. H., H. Thomas, K. Azetsu-Scott, B. J. W. Greenan, E. Head, and E. Horne (2011), Seasonal variability of dissolved inorganic carbon and surface water pCO_2 in the Scotian Shelf region of the Northwestern Atlantic, *Mar. Chem.*, *124*, 23–37, doi:10.1016/j.marchem.2010.11.004.

Shadwick, E. H., T. W. Trull, H. Thomas, and J. A. E. Gibson (2013), Vulnerability of polar oceans to anthropogenic acidification: Comparison of Arctic and Antarctic seasonal cycles, *Nat. Sci. Rep.*, *3*, 2339, doi:10.1038/srep.02339.

Siegel, D. A., S. C. Doney, and J. A. Yoder (2002), The North Atlantic spring phytoplankton bloom and Sverdrup's critical depth hypothesis, *Science*, *296*, 730–733.

Sutton, A. J., et al. (2014), A high-frequency atmospheric and seawater pCO_2 data set from 14 open ocean sites using a moored autonomous system, *Earth Syst. Sci. Data*, *6*, 353–366.

Sverdrup, H. U. (1953), On conditions for the vernal blooming of phytoplankton, *J. Cons. Int. Explor. Mer*, *18*, 287–295.

Sweeney, C., E. Gloor, A. R. Jacobson, R. M. Key, G. McKinely, J. L. Sarmiento, and R. Wanninkhof (2007), Constraining global air-sea gas exchange for CO_2 with recent bomb ^{14}C measurements, *Global Biogeochem. Cycles*, *21*, GB2015, doi:10.1029/2006GB002784.

Takahashi, T., et al. (2002), Global sea-air CO_2 flux based on climatological surface ocean pCO_2, and seasonal biological and temperature effects, *Deep Sea Res., II*, *49*, 1601–1622.

Takahashi, T., et al. (2009), Climatological mean and decadal changes in surface ocean pCO_2, and net sea-air CO_2 flux over the global oceans, *Deep Sea Res., II*, *56*, 554–577.

Takahashi, T., S. Sutherland, and A. Kozyr (2012), *Global Ocean Surface Water Partial Pressure of CO_2 Database: Measurements Performed During 1957–2012 (Version)*, Carbon Dioxide Information Analysis Center, Oak Ridge Natl. Lab., U. S. Dep. of Energy, Oak Ridge, Tenn., doi:10.3334/CDIAC/OTG.NDP088(V2012).

Taylor, J. R., and R. Ferrari (2011), Shutdown of turbulent convection as a new criterion for the onset of spring phytoplankton blooms, *Limnol. Oceanogr.*, *56*, 2293–2307.

Trull, T., S. R. Rintoul, M. Hadfield, and E. R. Abraham (2001), Circulation and seasonal evolution of polar waters south of Australia: Implications for iron fertilization of the Southern Ocean, *Deep Sea Res., II*, *48*, 2439–2466.

Trull, T. W., S. G. Bray, S. J. Manganini, S. Honjo, and R. Francois (2001), Moored sediment trap measurements of carbon export in the Subantarctic and Polar Frontal Zones of the Southern Ocean, South of Australia, *J. Geophys. Res.*, *106*, 31,489–31,510.

Wakita, M., S. Watanabe, A. Murata, N. Tsurushima, and M. Honda (2010), Decadal change of dissolved inorganic carbon in the subarctic western North Pacific Ocean, *Tellus B*, *62*, 608–620, doi:10.1111/j.1600-0889.2010.00476.x.

Wang, X., R. J. Materar, and T. W. Trull (2001), Modeling seasonal phosphate export and resupply in the Subantarctic and Polar Frontal Zones in the Australian sector of the Southern Ocean, *J. Geophys. Res.*, *106*, 31,525–31,541.

Wanninkhof, R. (1992), Relationships between wind speed and gas exhange over the ocean, *J. Geophys. Res.*, *97*, 7373–7382.

Watson, A. J., et al. (2009), Tracking the variable North Atlantic sink for atmospheric CO_2, *Science*, *326*, 1391–1393.

Weeding, B., and T. W. Trull (2014), Hourly oxygen and total gas tension measurements at the Southern Ocean Time Series site reveal winter ventilation and spring net community production, *J. Geophys. Res. Oceans*, *119*, 348–358, doi:10.1002/2013JC009302.

Weiss, R. F. (1974), Carbon dioxide in water and seawater: The solubility of a non-ideal gas, *Mar. Chem.*, *2*, 203–215.

Wong, C. S., and R. J. Matear (1999), Sporadic silicate limitation of phytoplankton productivity in the subarctic NE Pacific, *Deep Sea Res., II*, *46*, 2539–2555.